

pubs.acs.org/cm Article

# Multistep Regioselectivity and Non-Kirkendall Anion Exchange of Copper Chalcogenide Nanorods

Luis F. Garcia-Herrera, Haley P. McAllister, Huiyan Xiong, Haiying Wang, Robert W. Lord, Sarah K. O'Boyle, Adem Imamovic, Benjamin C. Steimle, Raymond E. Schaak, and Katherine E. Plass\*



Cite This: https://doi.org/10.1021/acs.chemmater.1c01107



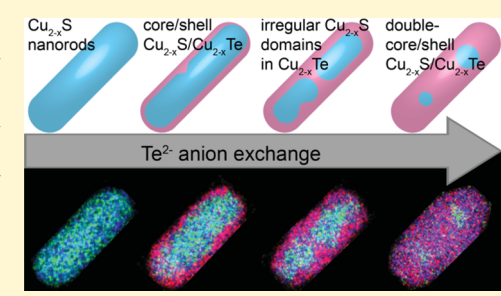
**ACCESS** 

III Metrics & More

Article Recommendations

Supporting Information

ABSTRACT: Chemical reactions that modify the compositions of nanoparticles are important for optoelectronic and catalytic applications. Understanding how they occur, and the unique features that can be produced as a result, is an important prerequisite to designing intricate nanostructures with complex morphologies. Here, we report the conversion of  $\alpha$ -chalcocite copper sulfide nanorods into weissite copper telluride nanorods through anion exchange. By examining the elemental composition, morphology, and crystallinity post exchange, it was found that the tellurium ions replaced sulfur ions to generate weissite in a way that maintained the (pseudo-)hexagonally close-packed sublattice as well as the morphology and crystallinity. Unusually, the anion exchange proceeded without inducing voids in the product nanoparticles. Such voids,



produced through the Kirkendall effect, are commonly observed during nanocrystal anion exchange reactions, yet can be important to avoid minimizing defects. The lack of void formation was explained by the balancing of inward and outward anion diffusion offered by nanoscopic pathways that formed within the nanorods at the early stages of the anion exchange reaction. The presence of these exchange-facilitating faults results in an unusual multistep process altering the locations at which copper telluride regions emerged during partial exchange. Three different anion movement regimes resulted in three distinct geometries. Initially, a nearisotropic exchange produced a copper sulfide/copper telluride core—shell structure. As the exchange progressed, the defect-mediated movement resulted in irregularly shaped copper sulfide domains within copper telluride. Phase segregation then led to a unique double-core copper sulfide/copper telluride heterostructure. This work offers insights into the mechanism behind anion exchange, highlights the design capabilities emergent from defective materials, and creates new opportunities for rational synthesis of complex nanoheterostructures.

ation exchange is a powerful and well-investigated avenue for transforming one nanoparticle (NP) into another, with the retention of morphology and crystal structure. In contrast, the possibilities for synthetic control afforded by anion exchange processes have not been thoroughly explored. Full and partial cation exchange processes routinely produce particles that retain shape and phase and generate complex nanoheterostructures.<sup>1–11</sup> Cation exchange has been explored in numerous systems, and the influence of many different variables has been elucidated. 4,12-18 Anion exchange, 18-20 in comparison, has been relatively limited due to lower ion mobility and the greater difficulty of exchanging the structural scaffold of larger anions without major perturbations of the initial particle. The slower diffusion of anions results in higher temperatures and longer reaction times for anion exchange than for cation exchange.<sup>20</sup> Reports of anion exchange are largely confined to a few systems. Metal halide perovskites, for example, 21-24 allow facile anion exchange under mild conditions due to their ionic character. Such a rapid anion movement enables a change from anion mixing under thermal conditions to phase segregation under irradiation.<sup>25,26</sup> The transformation of metal oxides to other metal chalcogenides by

anion exchange is usually accompanied by void formation due to the Kirkendall effect. The exchange of  $O^{2-}$  to softer chalcogenides ( $S^{2-}$ ,  $Se^{2-}$ , and  $Te^{2-}$ ) is promoted by the favorable soft—soft interactions with larger, lower valent cations.

There are few reports of interconversions of metal sulfide, selenide, and telluride NPs through anion exchange, yet such interconversions would afford a range of new phases, morphologies, and nanoheterostructures based on the well-developed syntheses of metal sulfides and selenides. This is especially important given that the direct solution synthesis of metal tellurides is often problematic due to the tendency to form tellurium oxide and the reactivity of many tellurium reagents.<sup>29</sup> One route around this difficulty is the trans-

Received: March 30, 2021 Revised: May 5, 2021



formation of metal to metal telluride NPs under mild conditions, albeit without morphology retention.  $^{29}$  In one example of the introduction of Te into a metal sulfide NP, Saruyama et al. converted CdS spheres to CdS–CdTe tear drops, affording a distinct CdTe crystal system and significant morphology alteration.  $^{30}$  This conversion was driven by the stronger TOP=S bond formed when  $\rm S^{2-}$  was removed from the particle to be replaced with Te²-, suggesting that their approach should be widely applicable. Two other prior reports of the conversion of copper sulfide or selenide to copper telluride resulted in significant changes to the shape  $^{31}$  or breaking up of the particles.  $^{32}$ 

Facile interconversion of nanoscale metal sulfides, selenides, and tellurides without morphology alteration represents a bottleneck in current postsynthetic transformations. Lim et al. assert that some sort of morphological perturbation during anion exchange is nearly inevitable.<sup>33</sup> This is due to the unequal diffusion rate between the incoming and outgoing ions that results in the Kirkendall effect.<sup>34</sup> Disproportionate mobilities produce voids when the outgoing ions diffuse more quickly than incoming ions or cracking when the opposite occurs.<sup>34</sup> Post-exchange products exhibiting voids or hollowed-out centers have been termed as having yolk/shell, core/shell, or core/sheath structures. <sup>27,35,36</sup> Comparably rapid rates of incoming anions versus outgoing anions result in the thorough fracture of rods<sup>37</sup> and plates.<sup>32</sup> Alterations such as these have been observed in nanoscale rods, tubes, spheres, sheets, and even tetrapods. 28,32,38-40 Notably, a report of anion exchange without the formation of Kirkendall voids occurred via careful alteration of the anion exchange chemistry to better match the mobilities of incoming and outgoing ions to switch off the Kirkendall effect.<sup>33</sup>

In addition to designing guidelines for avoiding Kirkendall voids, regioselective partial exchange is another crucial design tool, which can permit the creation of complex nanoheterostructures with manifold geometries by targeted replacement of certain atoms. Cation exchange can, broadly, create alloys, core-shell structures, or segmented structures. Depending on the lattice compatibility of the components involved, segmented structures can result in Janus particles, <sup>12,42</sup> sandwich shapes, <sup>14,43</sup> striped rods, <sup>2,44</sup> or tipped rods. <sup>44</sup> The combination of multiple partial exchanges can result in isomeric structures depending on the order of exchange due to differential regioselectivity. 16 The existing interfaces can also promote exchange, resulting in a large variety of striped rods with multiple chemical domains. <sup>1</sup> Cation exchange can also proceed through distinct phases where initial random exchange evolves into new phase-segregrated structures.<sup>44</sup> Theoretically, similar design principles should be applicable to anion exchange, but there are few examples of complex geometries resulting from anion exchange. Core-shell particles regularly formed as metal oxides undergo anion exchange, typically ending as void-containing shapes. 27,39 CsPbBr3 nanocubes can undergo anion exchange either homogeneously or through the formation of isotropic zones, depending on the halogen exchanged.<sup>22</sup>

Here, we report the transformation of copper-deficient copper sulfide  $(Cu_{2-x}S)$  nanorods to copper telluride  $(Cu_{2-x}Te)$  through anion exchange (Figure 1a), giving rise to nanorods with complex geometries without voids. The transformation procedure was modeled on that used by Saruyama et al.,<sup>30</sup> wherein the precursor particles suspended in oleylamine were exposed to a solution of Te=TOP complex.

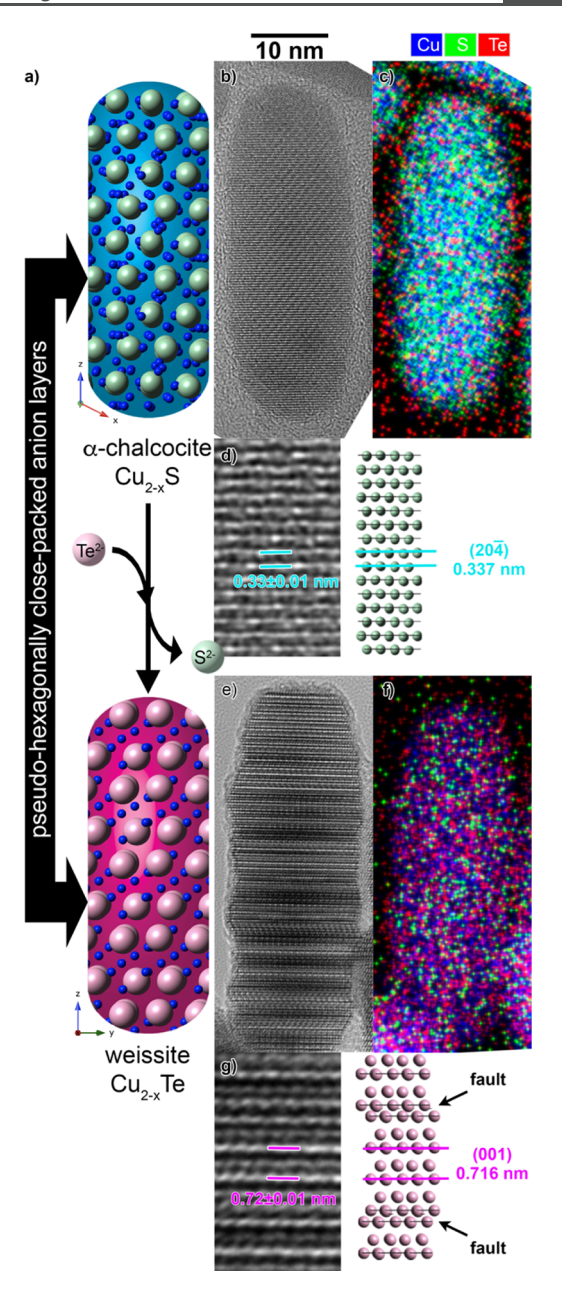


Figure 1. Representation of the anion exchange process (modeled on published schemes  $^{10,11}$ ) with the comparison of the crystal structures of  $\alpha$ -chalcocite and trigonal weissite, illustrating the planes apparent in the HR-TEM and their orientation with respect to the rods (a). HR-TEM and EDS maps of copper sulfide nanorods before (b-d) and after (e-g) Te exchange, showing the change in chemical composition, and alteration in crystal structure, with a zoomed-in comparison to the crystal structure (d,g).

The anion exchange proceeds without Kirkendall void formation through a process that is fundamentally different than that previously reported;  $^{33}$  stacking-fault defects within the nanorods serve as conduits for anion transport, thereby equalizing inward and outward diffusion. The creation of fully exchanged  $\mathrm{Cu}_{2-x}\mathrm{Te}$  rods without altered morphology or void formation opens up avenues for exploring this useful material, as well as applying the anion exchange pathway to other compounds. Copper telluride, in particular, exhibits nearinfrared plasmonic behavior  $^{45-47}$  and has applications in electrocatalysis  $^{31}$  and thermoelectrics.  $^{48-50}$  Partial anion

exchange produced distinctive double-core geometries and revealed a complex evolution of  $\mathrm{Te^{2^-}}$  position that provided insights into the kinetics of anion movement. Three distinct anion movement stages were identified, including a defect-mediated stage that was essential for the formation of complex geometries.

## 2. EXPERIMENTAL SECTION

- **2.1. Chemicals.** The reagents used for the synthesis of roxbyite NPs include copper nitrate dihydrate  $(Cu(NO_3)_2\cdot 3H_2O, 99.95\%)$ , copper acetylacetonate  $(Cu(acac)_2, 99.9\%)$ , sulfur powder (99.98%), trioctylphosphine (TOP) oxide  $(\geq 90\%)$ , oleylamine (technical grade, 70%), 1-octadecene (technical grade, 90%), tert-dodecyl mercaptan (mixture of isomers, 98.5%), and 1-dodecanethiol  $(\geq 98\%)$ . Additional reagents used for the cation exchange include cadmium(II) acetate dihydrate  $(Cd(OAc)_2\cdot 2H_2O, 99.999\%$  trace metal basis), dibenzyl ether (99%), and TOP  $(\geq 85\%)$ . All solvents used for the precipitation and washing of NPs, including isopropyl alcohol (IPA), toluene, hexane, and acetone, were of analytical grade. Unless specified, all reagents were purchased from Sigma-Aldrich and used as received.
- **2.2. General Safety Concerns.** The synthetic methods in this report are performed under air-free conditions at elevated temperatures using high-boiling-point solvents. As such, care should be taken to ensure proper monitoring and handling. For example, burns have been reported from exposure to high-temperature oleylamine. The safety data sheets for all chemicals used in the reactions should be reviewed, and proper personal protective equipment should be used. These reactions have the potential to evolve toxic gases and as such should be handled in a properly functioning fume hood.
- **2.3. Standard Reaction Vessel Setup.** Each of the following procedures utilizes either a standard Schlenk line setup or an Ar gas manifold. Each three-necked, round-bottom flask was equipped with a magnetic stir bar, a reflux condenser with a glass adaptor connected either to the Schlenk line or to a bubbler, a type-K thermocouple through a silicone septum, and a second septum with a needle to connect to the Ar gas. The temperature was controlled by heating the mantles on magnetic stir plates.
- 2.4. Synthesis of Copper Sulfide Nanorods. Cu<sub>18</sub>S nanorods were synthesized in 40% yield using an adaptation of previously published procedures.<sup>8,51</sup> The synthesis was performed using a Schlenk line setup. Cu(NO<sub>3</sub>)<sub>2</sub>·3H<sub>2</sub>O (281 mg), TOP oxide (2.9 g), and octadecene (15 mL) were combined in a 50 mL three-neck flask and placed under vacuum. This mixture was degassed at 80  $^{\circ}$ C for 30 min, resulting in a blue solution. After the degassing period, the flask containing the copper precursor was cycled with Ar and vacuum three times, with each cycle lasting 5 min. The flask was then placed under a blanket of Ar, and the reaction temperature was increased to 180 °C. As the temperature was increased, 15 mL of the degassed 10:1 mixture of tert-dodecyl mercaptan/1-dodecanethiol was rapidly injected at 135 °C, resulting in a yellow-colored solution. As the temperature begins to increase, the reaction mixture will follow the following color changes in order: yellow, orange, yellow, orange, dark orange/brown, dark brown. When the temperature reaches 180 °C, the solution will become dark brown but not turbid, indicating the formation of Cu<sub>2-x</sub>S NPs. After the solution became turbid (typically after 5 min), the flask was then held at this temperature range for 15 min to allow for the one-dimensional growth of the Cu<sub>1.8</sub>S nanorods. After the growth time, the flask was cooled rapidly by removing the heating mantle and placing the flask into a room-temperature water bath. Toluene (40 °C, 2 mL) was injected into the reaction mixture. The resulting product was precipitated with 20 mL of IPA, followed by centrifugation for 10 min at 6000 rpm and resuspension in 5 mL of hexane. The particles were then washed two more times with a 1:1 ratio of IPA/acetone, with three drops of oleylamine added between the first wash and the second wash. The final brown product was resuspended in 5 mL of hexane for characterization and use in further reactions.

- 2.5. Tellurium Exchange Procedure. The Te exchange procedure was modeled on that published by Saruyama et al.<sup>30</sup> and carried out with 80% yield. The transformation was performed using an Ar gas manifold. TOP telluride (TOP=Te) was prepared from a mixture of elemental Te (0.0383 g, 0.3 mmol), 1-octadecene (5 mL), and TOP (1.2 mL) combined in a 25 mL three-neck flask. The flask must be placed in a blanket of Ar before injecting TOP. The reagents were stirred at 240-260 °C under dry Ar until all elemental Te disappeared (~15-20 min) to form a translucent yellowish solution. The resulting solution was heated to 260 °C or to a desired temperature for exchange. A suspension of  $Cu_{x-2}S$  NPs in hexane (4 mL of ~5 mg/mL to give 0.0200 g) was air-dried in a septum-capped vial and then oleylamine (4 mL) was added. The vial was then placed under an Ar blanket for 5 min and then parafilmed and sonicated for 10 min to disperse the particles. The NPs/oleylamine solution was then swiftly injected into TOP=Te. The solution was left to exchange between 10 min and 1 h. After the reaction, the reaction flask was cooled to room temperature, washed with ethanol (20 mL), and centrifuged to isolate the NPs as black precipitates. A second wash and third wash were carried out with a 4:1 ratio of ethanol/hexane. The precipitates were suspendable in nonpolar solvents such as hexane and toluene.
- **2.6. Characterization.** 2.6.1. Powder X-Ray Diffraction. After the NPs were cleaned and resuspended in hexane, they were cast onto glass slides and allowed to dry and then covered with Parafilm to avoid exposure to solid NPs. The powder X-ray diffraction (PXRD) data were collected using a PANalytical X'Pert Pro X-ray diffractometer with Cu K $\alpha$  radiation. The samples were scanned with 10 repetitions at a current of 40 mA and voltage of 45 kV. Using the PANalytical HighScore Plus software, the 10 scans were summed and the peaks were compared with the patterns from the ICDD database to determine the structure of the NPs. Crystal structure and powder diffraction simulations were performed using CrystalMaker and CrystalDiffract from CrystalMaker Software Ltd., Oxford, England.
- 2.6.2. Transmission Electron Microscopy. Samples were prepared by placing a drop of NP suspension in hexane or toluene on a Nisupported ultrathin carbon-coated transmission electron microscopy (TEM) grid (Electron Microscopy Sciences). The TEM images of the particles and their average sizes were obtained using one of the two microscopes, a Delong Instruments LVEM25 Low-Voltage TEM at Franklin & Marshall College or the FEI Tecnai G20 20 XTWIN at the Materials Characterization Laboratory at the Pennsylvania State University. LVEM25 was operated under 25 kV with the Zyla 5.5 Scientific CMOS camera with appropriate alignments and enhancements. ImageJ software was used to analyze the TEM images.
- 2.6.3. Scanning Electron Microscopy/Energy-Dispersive X-ray Spectroscopy. NPs suspended in hexane were allowed to dry and then uniformly immobilized on a small piece of conductive carbon tape. Scanning electron microscopy (SEM) and energy-dispersive X-ray spectroscopy (EDS) of the sample were then carried out at 20 kV with the Evex Mini-SEM system.
- 2.6.4. High-Angle Annular Dark-Field Scanning Transmission Electron Microscopy/EDS Mapping. Samples were prepared by placing a drop of NP suspension in hexane or toluene on a Nisupported ultrathin carbon-coated TEM grid (Electron Microscopy Sciences). The microscope employed was an FEI Talos F200X with a SuperX EDS at 200 kV in the Materials Characterization Laboratory at the Pennsylvania State University. ImageJ software was used to analyze the high-resolution transmission electron microscopy (HR-TEM) images. Bruker ESPIRIT 2 software was used to interpret the scanning transmission electron microscopy (STEM)—EDS element map data.

# 3. RESULTS AND DISCUSSION

3.1. Demonstration of Anion Exchange with the Retention of Morphology. Exposure of  $\alpha$ -chalcocite copper sulfide (Cu<sub>2-x</sub>S) nanorods to a Te=TOP solution at a high temperature and extended times (260 °C for more than 1 h)

resulted in the transformation of copper sulfide rods to copper telluride, with the retention of morphology and crystallographic features (Figure 1a,b). TEM-EDS shows that the chemistry changes from  $Cu_{2-x}S$  (Cu/S 1.71  $\pm$  0.04) to  $Cu_{2-x}$ Te (Cu/Te 1.53  $\pm$  0.07), as mirrored in the EDS maps shown in Figure 1c,f. This Cu/Te ratio is consistent with the calculations and literature reports of weissite copper telluride, with stoichiometries from Cu<sub>2</sub>Te to Cu<sub>2.98</sub>Te<sub>2</sub>. <sup>52</sup> The residual S measured is  $1.2 \pm 0.5$  atomic %, which is near the detection limit for EDS (Figure S1). The removal of a small amount of Cu is consistent with the etching of copper sulfide by TOP in the presence of trace oxygen<sup>8,53</sup> and can be accommodated by the flexibility in stoichiometry exhibited by copper chalcogenides. Nanorod morphologies were retained upon anion exchange, which is crucial for distinguishing postsynthetic transformation from direct synthesis (Figure 2c-f). Particles

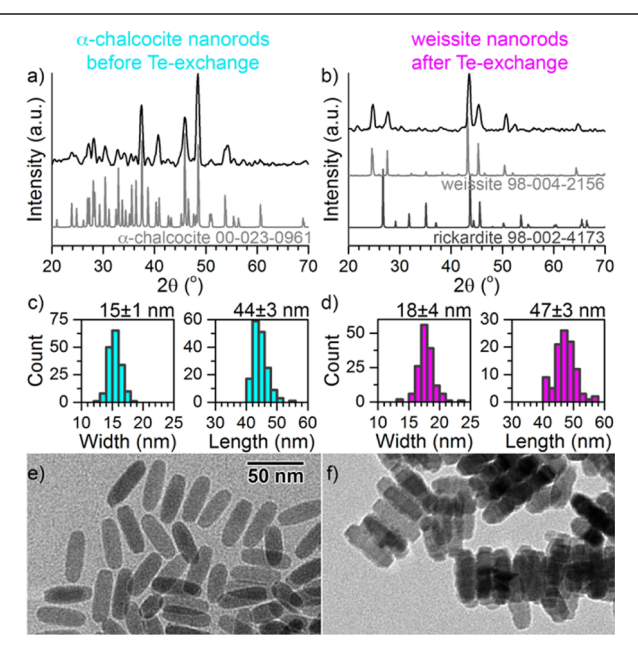


**Figure 2.** PXRD patterns before (a) and after (b) Te exchange support the identification of  $\alpha$ -chalcocite and weissite phases. Histograms of length and width measured from the representative assemblies of particles before (c,e) and after (e,f) Te exchange, showing the change in phase from  $\alpha$ -chalcocite to weissite without a statistically significant change in particle size or shape.

did exhibit greater aggregation after exchange, suggesting some removal of surface ligands. Prior to exchange, the rods have lengths of  $58 \pm 3$  nm and widths of  $21 \pm 1$  nm with smooth surfaces (Figure 2c,e). After Te exchange, the rod lengths altered slightly to  $61 \pm 5$  nm and width to  $23 \pm 1$  nm in (Figure 2d,f). This expansion is within the error of the particle size measurements and the degree of expansion expected upon comparison of the crystal structures (Figure S2). This retention of morphology is distinct from prior reports of conversion from copper sulfide to copper telluride, which showed marked shape alteration and even breakdown of the particles along the exchange pathways.

The retention of the anion sublattice and crystallographic orientation further supports that copper telluride is generated through the anion exchange of copper sulfide. The  $\alpha$ -chalcocite copper sulfide nanorods transform to trigonal weissite copper telluride, with the retention of the pseudohexagonally closepacked anion sublattice structure (Figure 1a). PXRD (Figure

2a,b) shows the transformation of  $\alpha$ -chalcocite nanorods to a weissite structure. Before exchange, the PXRD pattern exhibits major reflections due to the  $\alpha$ -chalcocite phase, a monoclinic phase with a pseudohexagonally close-packed sulfide sublattice (Figure 1a). The PXRD pattern before exchange shows major peaks due to the sulfide sublattice at 46.9 and  $48.8^{\circ}$   $2\theta$  as well as many lower intensity peaks due to complex cation ordering distinctive of the  $\alpha$ -chalcocite phase (Figure 2a). Both roxbyite and  $\alpha$ -chalcocite were formed in the copper sulfide nanorod synthesis process; these structures vary slightly in stoichiometry and cation ordering (Figure S3) but share the placement of cations in primarily trigonal holes. Roxbyite contains additional Cu ions in tetrahedral holes. Telluride exchange was also successful for roxbyite rods (Figure S4), which share a pseudohexagonal sulfide sublattice with  $\alpha$ -chalcocite. The PXRD pattern after Te exchange is distinguished by reflections at 24.7, 27.6, 43.5, and 45.5°  $2\theta$  (Figure 2b). The observed relative peak intensities are best attributed to the trigonal weissite structure (see Supporting Information for further discussion, Figure S5), which is calculated to be the most stable phase at this  $Cu_{15}$ Te stoichiometry. The  $\alpha$ -chalcocite copper sulfide phases are structurally analogous to trigonal weissite copper telluride (Figure 1a). In both the copper sulfide and copper telluride structures, S<sup>2-</sup> or Te<sup>2-</sup> anions are (pseudo-)hexagonally close-packed, while the cation positions differ substantially. As the structure transforms to weissite, the Cu ions shift position into exclusively tetrahedral holes. In cation exchange, the starting particle influences the crystallographic orientation of the incoming phase, consistent with the slow replacement of ions. 6,16,54 The same behavior is seen here for anion exchange. HR-TEM images show that the initial  $\alpha$ chalcocite rods are oriented such that the close-packed anion planes (the  $\{20\overline{4}\}\$ planes) are perpendicular to the sides of the rods. Before exchange, the spacing of planes propagating along the length of the rod is  $0.33 \pm 0.01$  nm (Figure 1d), consistent with the spacing between the close-packed planes of 0.337 nm (Figures 1a and S2). After exchange (Figure 1e,g), the weissite rods show prominent planes along the length of the rod with similar spacing as for the  $\alpha$ -chalcocite rods but with frequently alternating contrast (Figure 1g). In areas where the alternating contrast is consistent, a spacing of  $0.72 \pm 0.01$  nm is measured, corresponding to the 0.716 nm spacing between the {001} planes of trigonal weissite. This difference in contrast is consistent with the formation of trigonal weissite. In trigonal weissite, the close-packed Te<sup>2-</sup> layers are not evenly spaced but instead form pairs of layers separated by more Cu-rich regions. There are many defects in this alternating contrast pattern (Figure 1g). Such semiperiodic disruptions of stacking planes could be attributed to stacking faults or polytypism,<sup>55</sup> though similar patterns can be induced by stress due to lattice mismatch.<sup>56</sup> If the contrast differences are not considered, a periodicity of  $0.36 \pm 0.05$  nm is measured, consistent with the spacing of 0.358 nm between the close-packed {002} planes of the trigonal weissite structure. We propose that defects perpendicular to the side of the rod are introduced during the exchange process as anions move along these planes (a process supported by the analysis of partial exchange, vide infra). Based on the layered bonding pattern for weissite, shifting of the close-packed anion planes could occur with minimal disruption to the overall crystal structure. Such defects would also explain the lack of preferred orientation exhibited in the PXRD pattern for weissite (Figure 2b). This would also produce the striations observed in the low-magnification TEM

images (Figure 1e) as well as the increased surface roughness due to the shifting planes of close-packed anions (Figure 2f). Etching of the copper sulfide starting material by TOP may further contribute to surface roughness.<sup>8,53</sup>

It is unusual to observe anion exchange with so little perturbation of the morphology and without Kirkendall void formation as we have in this  $Cu_{2-x}S/Cu_{2-x}Te$  system. Though the size and aspect ratio are maintained, the fully exchanged Cu2-xTe rods show distinctly rougher edges and an increased number of striations in contrast, indicative of defects or polytypism,<sup>55</sup> but not central voids observed with the Kirkendall effect. Key to such notable retention of morphology is the balancing of the inward and outward anion diffusion rates.<sup>34</sup> The importance of this balance is emphasized by a recent report of modulation of the Kirkendall effect.<sup>33</sup> We propose that the retention of morphology here can be attributed to the synergy of several crystallographic features modulating the anion mobilities. The increase in the anion size of  $Te^{2-}$  versus  $S^{2-}$  suggests that, based on ion size alone,  $Te^{2-}$ should be less mobile in the crystal structure than S<sup>2-</sup>, though this differential is less than that expected for metal oxides transforming to metal sulfides. The increase in the anion size from  $S^{2-}$  (1.84 Å) to  $Te^{2-}$  ion (2.21 Å, increase of 0.37 Å) is slightly smaller than that observed when O2- (1.4 Å in VI coordination) is replaced with S<sup>2-</sup> (1.84 Å, increase of 0.44 Å).<sup>57</sup> Furthermore, based on the comparison of the  $\alpha$ chalcocite and weissite structures, the unit cell expands due to the increased size of the Te<sup>2-</sup> ion by 6.3% along the length of the rod and 5.1% across the diameter (Figure S2). The stoichiometry of the nanorods is altered from Cu<sub>1.7</sub>S to Cu<sub>1.5</sub>Te. The net removal of Cu during the anion exchange, indicated by the reduction in the overall Cu/anion ratio as well as the occasional observation of copper sulfide impurities (Figures 6d and S11), may aid morphology retention as well as

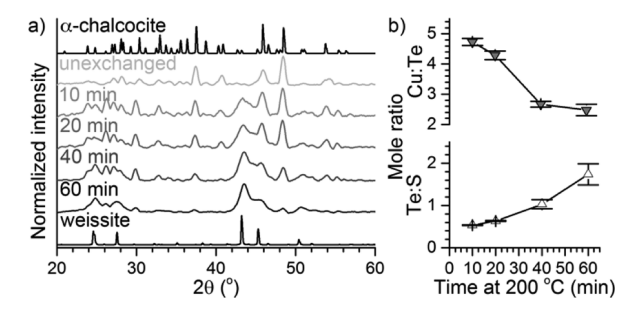


**Figure 3.** α-Chalcocite copper sulfide nanorods after exposure to Te=TOP at 200 °C for varying times, creating  $Cu_{2-x}S/Cu_{2-x}Te$  core/shell structures. The evolution with time is monitored through PXRD (a) and elemental composition (b).

transport and accommodation of the larger Te<sup>2-</sup> ions. The entry of Te<sup>2-</sup>, concurrent with the removal of Cu<sup>+</sup> and S<sup>2-</sup>, likely creates a situation in which the lattice is less likely to be overly strained and broken. Movement of the already highly mobile Cu<sup>+</sup> ions within the cation layers could create pathways for the exchange of S<sup>2-</sup> and Te<sup>2-</sup> that equalize the differences due to anion size. Lastly, these pathways perpendicular to the side of the rods could be further promoted by the crystalline defects that appear along the hexagonally close-packed anion planes that increase after anion exchange (Figure 1g). As noted above, semiperiodic disruptions to the crystal structure consistent with polytypism are prominent and common in

the exchanged rods. The coincidence of these disruptions with the close-packed layers could further accelerate anion motion.

**3.2.** Anion Exchange Shows Evolving Regioselectivity with Time and Temperature. Alteration in the time and temperature at which copper sulfide rods are exposed to the Te=TOP exchange solution results in partial exchange with tunability in the extent of exchange, crystallinity, and relative position of  $Cu_{2-x}S/Cu_{2-x}Te$  domains. Two regimes are explored in detail. At relatively low temperatures (200 °C),  $Cu_{2-x}S/Cu_{2-x}Te$  core/shell structures are observed. With alterations in temperature (200–260 °C for 1 h), we see greater alterations in the extent of exchange and crystallinity, as well as the relative position of copper sulfide and telluride.

3.3. Low Times and Temperature Produce Core-shell **Structure.** Anion exchange at 200 °C produced a Cu<sub>2-x</sub>S/ Cu<sub>2-x</sub>Te core/shell structure. After 10 min of exchange, PXRD shows the coexistence of crystalline weissite and lpha-chalcocite (Figure 3a), and EDS shows the presence of Te (1.4:0.55:1 Cu/Te/S) (Figure 3b). EDS mapping shows that Te is localized on the outside of the particles (Figures 4a, S6). When considering the possible regioselectivity resulting from ion exchange 41 for Cu<sub>2-x</sub>S/Cu<sub>2-x</sub>Te heterostructures, the formation of a core/shell geometry rather than an alloy is striking. While the large ion size difference between the sulfide and telluride prevents the sulfide-telluride alloy formation in chalcopyrite systems, 58 the direct synthesis of cubic Cu<sub>2-x</sub>S<sub>v</sub>Te<sub>1-v</sub> NPs has been reported at the moderate reaction temperatures employed here. Shell formation on rods that could accommodate alloy formation has been observed in the Se<sub>x</sub>Te<sub>y</sub>/Te core/shell system. 56 Two features are notable in the distribution of Te within the particle. The  $Cu_{2-x}$ Te shell on the sides of the rod is thicker than the shell at the tips, indicating enhanced growth perpendicular to the rod. Furthermore, the  $Cu_{2-x}$ Te shell is consistently thicker at one tip than the other. This is consistent with the noncentrosymmetric crystal structure, where the S-terminated tip and the Cu-terminated tip are likely to allow adsorption and anion exchange at different rates (Figure 1a).

As the anion exchange time at 200 °C increases, the  $Cu_{2-x}$ Te shell grows. As more Te is incorporated, EDS (Figure 3b) shows that the Cu/Te ratio steadily decreases (from 4.7  $\pm$ 0.1 for 10 min to 2.5  $\pm$  0.02 at 1 h) and the Te/S ratio steadily increases (from  $0.537 \pm 0.007$  for 10 min to  $1.7 \pm 0.3$  at 1 h). Despite this increase in shell thickness, particles exchanged at 200 °C remain well dispersed (Figure S7), unlike particles exchanged at 260 °C that lose a significant number of surface ligands. PXRD (Figure 3a) shows that the crystalline component steadily shifts from  $\alpha$ -chalcocite to weissite, as indicated by the change in the relative intensities. At 10 min, the most intense peak is that at  $45.5^{\circ}$   $2\theta$ , characteristic of a  $\alpha$ chalcocite peak. As time progresses, the  $45.5^{\circ}$   $2\theta$  peak shrinks while the peak at  $43.5^{\circ}$   $2\theta$ , indicative of weissite, dominates. After 1 h of reaction, the  $45.5^{\circ}$   $2\theta$  peak is just barely visible, indicating that the vast majority of the crystalline component is weissite, though significant amounts of copper sulfide remain in the EDS maps (Figure 4a). Over this same time, EDS maps show that the shell thickness gradually increases  $(4.9 \pm 0.9 \text{ nm})$ at 10 min,  $4.1 \pm 0.8$  nm at 20 min, and  $7 \pm 1$  nm at 40 min).

A close comparison of the EDS maps and HR-TEM images of the  $Cu_{2-x}S/Cu_{2-x}Te$  core/shell structures obtained at 200 °C (Figures 4a–d and S8 for additional images) reveals that the core/shell structures progress through an irregular propagation of  $Cu_{2-x}Te$  into the rods. The EDS maps show

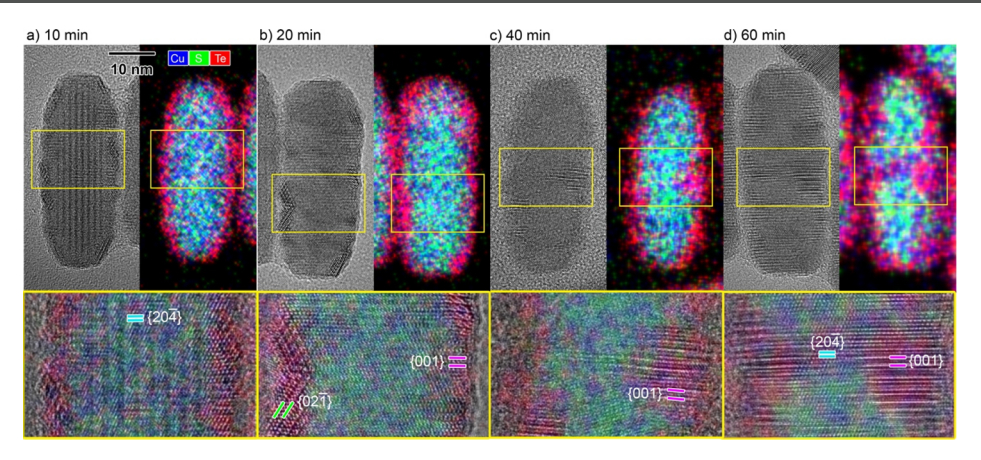


Figure 4.  $\alpha$ -Chalcocite copper sulfide nanorods after exposure to Te=TOP at 200 °C for varying times, comparing the HR-TEM and EDS maps, with the inset showing a magnified area overlaid with the EDS map. There is a correspondence between the appearance of Te (red in EDS) forming a shell around the nanorod and the crystallographic features indicative of trigonal weissite ({001} planes, magenta lines; {02 $\overline{1}$ } planes, green lines). The core of the nanorod retains S (green in EDS) and the {20 $\overline{4}$ } planes of  $\alpha$ -chalcocite (cyan lines).

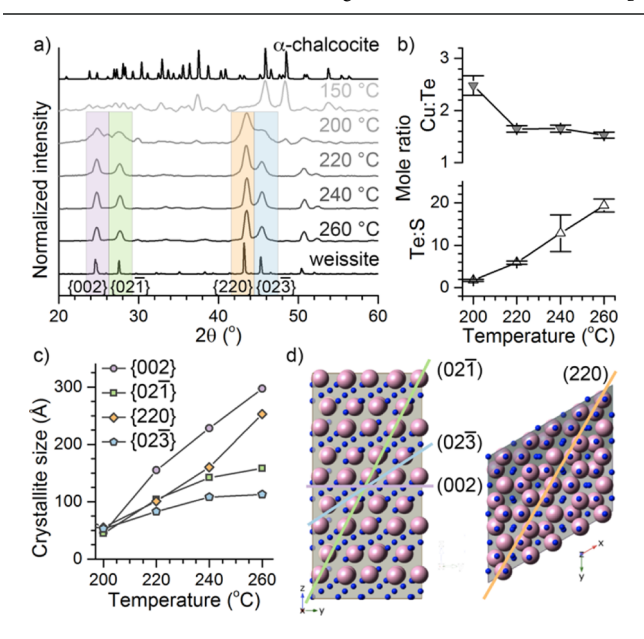


Figure 5.  $Cu_{2-x}S/Cu_{2-x}Te$  heterostructured nanorods after the exposure of  $\alpha$ -chalcocite copper sulfide nanorods to Te=TOP for 1 h at varying temperatures. The evolution with temperature is monitored through PXRD (a) and elemental composition (b). Scherrer analysis (c) reveals that the crystallinity increases dramatically with increasing temperature, both along the length (corresponding to the (002) planes) and width (corresponding to the (220) planes) of the rod (d).

a continuous shell of  $Cu_{2-x}Te$ , but some regions on the sides of the rods are thicker and even start to extend into the rod at later times (Figure 4c,d). The regions of  $Cu_{2-x}Te$  show increased contrast in the HR-TEM images (Figure 4a–d), with doubled spacing (0.72 nm, magenta lines) due to the trigonal weissite {001} planes, which maintain continuity with the remaining  $Cu_{2-x}S$  lattice (0.34 nm due to the  $\{20\overline{4}\}$   $\alpha$ -chalcocite planes shown in cyan). At early times,  $Cu_{2-x}Te$  can manifest as an "indented" region (Figure 4b) due to faceting with the  $\{02\overline{1}\}$  weissite planes (green lines), while later times (Figure 4c,d) exhibit the striated contrast pattern, consistent with the fully exchanged particle due to the  $\{001\}$  weissite planes with frequent stacking defects. Such defects could provide sites for increased  $Te^{2-}$  attachment as well as  $S^{2-}$ 

removal that would facilitate exchange at that point. It is notable that these disrupted areas are crystalline and often continuous with the lattice of the  $Cu_{2-x}S$  core. With increasing temperature, regioselective exchange evolves to form a coreshell, then irregular domains, and then double-core structures.

Anion exchange typically requires much higher temperatures than cation exchange, which can proceed even at room temperature. This necessity allows fine-tuning of behavior over a large range of temperatures, resulting in different extents of exchange and geometries. The attempted exchange at 150 °C for 1 h did not result in an appreciable exchange of  $S^{2-}$  for  $Te^{2-}$ . PXRD (Figure 5a) shows only  $\alpha$ -chalcocite reflections, while EDS indicates that a near-zero amount of Te has been introduced. Exchange between 200 and 260 °C, however, resulted in a rich array of different nanoheterostructures.

While Te exchange at 200 °C for less than 1 h resulted in  $Cu_{2-x}S/Cu_{2-x}Te$  core/shell structures, the evaluation of the exchange at 1 h across a range of temperatures revealed increased exchange and different placements of Cu2-xS within a primarily Cu<sub>2-x</sub>Te rod. PXRD of nanorods exchanged at or above 200 °C for 1 h showed complete disappearance of the initial  $\alpha$ -chalcocite phase and transformation of the crystalline component of the nanoheterostructure to copper telluride (Figure 5a). The extent of Te<sup>2-</sup> incorporation increased steadily from a 1.7  $\pm$  0.3 mol ratio of Te/S at 200 °C to a 19  $\pm$ 1 mol ratio of Te/S at 260 °C (Figure 5b). Note that only samples without the contamination such as that shown in Figure 6d were included in the determination of the mole ratio. The Cu/Te ratios approach the final value of 1.5  $\pm$  0.1, which is within the standard deviation of the value observed for complete exchange at 260 °C over 2 h (Cu/Te 1.53  $\pm$  0.07). The crystalline domain size for copper telluride increases with temperature, as shown by the width of the diffraction peaks. Scherrer analysis (Figure 5c) shows that the crystallinity along the {002} planes, which run the length of the rods (Figure 5d), increases most dramatically, with the maximum crystallite size of 30 nm roughly equal to the distance between the double cores of copper sulfide  $(24 \pm 6 \text{ nm})$ . Such an increase in crystallinity is reflected in the HR-TEM behavior (Figure 6). At 220 °C (Figure 6b) and 240 °C (Figure 6c), the areas corresponding to the copper sulfide cores appear continuous with the surrounding crystal, while the highly crystalline particles achieved at an exchange temperature of 260 °C

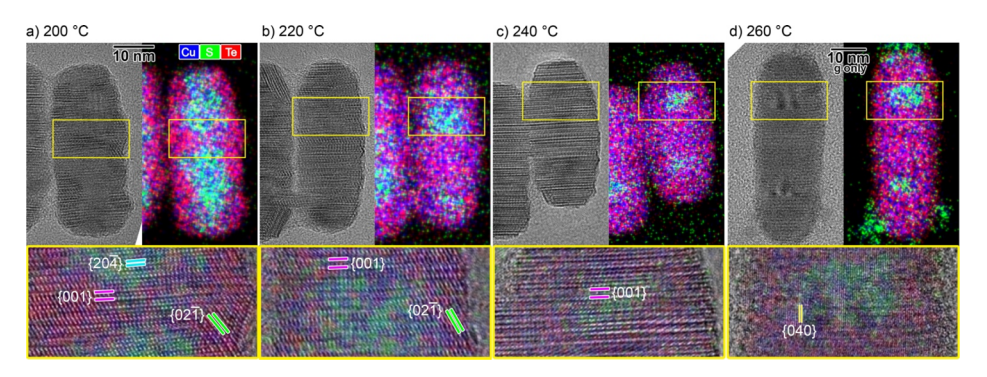


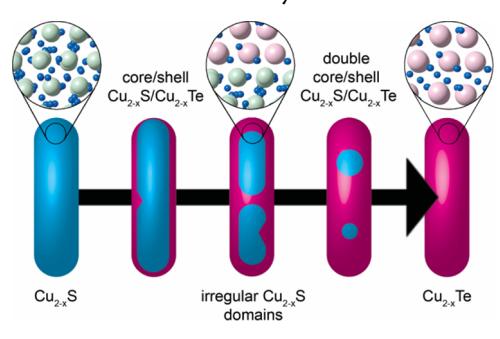
Figure 6.  $Cu_{2-x}S/Cu_{2-x}Te$  heterostructured nanorods after the exposure of α-chalcocite copper sulfide nanorods to Te=TOP for 1 h at varying temperatures. α-Chalcocite copper sulfide nanorods after exposure to Te=TOP at 200 °C for varying times, comparing the HR-TEM and EDS maps, with the inset showing a magnified area overlaid with the EDS map. There is a correspondence between the appearance of Te (red in EDS) forming a shell around the nanorod and the crystallographic features indicative of trigonal weissite ( $\{001\}$  planes, magenta lines;  $\{02\overline{1}\}$  planes, green lines;  $\{040\}$  planes, yellow lines). The core of the nanorod retains S (green in EDS) and the  $\{20\overline{4}\}$  planes of α-chalcocite (cyan lines). The particular sample shown in (d) reveals that sulfur-rich copper sulfide is formed in solution, though it is usually washed away.

(Figure 6d) show strain induced by the mismatch of the ion sizes. The {220} planes have a maximum domain size of 25 nm that roughly corresponds to the width of the particles.

EDS mapping and HR-TEM (Figure 6a-d) show how the placement of Cu<sub>2-x</sub>S and Cu<sub>2-x</sub>Te within the rod evolves with temperature. While early times at 200 °C (Figure 4a-c) showed Cu<sub>2-x</sub>S/Cu<sub>2-x</sub>Te core/shell structures, after 1 h, stripes of Cu2-xTe appear perpendicular to the side of the rod (Figures 4d and 6a), breaking up the  $Cu_{2-x}S$  core into a variable number of irregular domains. The examination of EDS maps of many nanorods exchanged for 1 h at 200 °C (Figure S8) shows a mixture of extents of stripe formation. Of these 18 nanorods, there exist five wherein the Cu<sub>2-x</sub>S domain has been broken by a stripe of Cu<sub>2-x</sub>Te that extends across the whole particle. Others show divots of  $Cu_{2-x}$ Te in  $Cu_{2-x}$ S. These same  $Cu_{2-x}$ Te areas correlate to the areas of alternating contrast in the HR-TEM images due to the trigonal weissite {001} (magenta lines) or  $\{02\overline{1}\}$  planes (green lines) (Figures 4d and 6a). Particles exchanged at 220 °C for 1 h (Figure 6b) show continued progression of Cu2-xTe from the sides of the rod encroaching on the Cu<sub>2-x</sub>S core until most particles (all 15 of the different particles imaged in Figure S9) have multiple domains of Cu<sub>2-x</sub>S irregularly placed along the rod. HR-TEM confirms that the crystallinity of the rod, overall, is maintained, though the distinction between the planes of weissite and  $\alpha$ chalcocite becomes difficult as weissite surrounds Cu<sub>2-x</sub>S in three dimensions. As the crystallinity increases with temperature, the rods exchanged at 260 °C (Figure 6d) show that the areas corresponding to the Cu<sub>2-x</sub>S domains in the EDS maps exhibit variations in contrast, consistent with the strain induced by the lattice mismatch between  $Cu_{2-x}S$  and  $Cu_{2-x}Te$ . Te exchange at 240 and 260 °C for 1 h results in the coalescence of  $Cu_{2-x}S$  domains, typically into two cores of  $Cu_{2-x}S$  offset at either end of the rod, though there are a few examples of one offset Cu<sub>2-x</sub>S core or one central Cu<sub>2-x</sub>S core. This doublecore pattern is remarkably consistent. Figures S10 and S11 show 18 different rods, with the position of  $Cu_{2-x}S$  placed at either end of 16 of the 18 rods, though the prominence and position change slightly between the rods. The continuous lattice fringes observed through HR-TEM analysis in Figure 6 reinforce the conclusion that the copper sulfide cores are embedded within the copper telluride rod, with an epitaxial interface between the two crystalline regions of copper sulfide and copper telluride. The center of each core is roughly onequarter of the length of the rod from each end ( $26 \pm 9\%$  of the rod length measured across all 16 rods). The 260 °C samples occasionally showed deposited copper sulfide that is of low crystallinity and attached to the surface, which serves as a useful comparison with the copper sulfide double cores embedded in the copper telluride rods. The copper sulfide cores show continuous crystal planes with copper telluride, with the alterations in contrast attributable to the strain due to mismatched lattice spacings. This observation of copper sulfide outside of the rod, coupled with a net decrease in the Cu/chalcogenide ratio, supports the supposition that there is a net removal of Cu<sup>+</sup> ions which could aid the incoming and outgoing anion mobilities.

Upon examination of the evolution in regioselectivity of the  $Cu_{2-x}S/Cu_{2-x}Te$  heterostructures formed by anion exchange, we propose a three-stage process (Scheme 1). In the first stage,

Scheme 1. Three-Stage Process that Describes the Evolution in Regioselectivity of  $Cu_{2-x}S/Cu_{2-x}Te$ Nanoheterostructures Formed by  $Te^{2-}$  Anion Exchange



core—shell particles form as incoming  $Te^{2-}$  anions travel nearly isotropically from the outside of the particle. The shells show nonuniformities, indicating rapid exchange along the walls of the rods in general, with the areas of surface disruption showing further accelerated exchange. The chemistry of one tip is also more amenable to anion exchange. In the second stage,  $Te^{2-}$  anion movement is accelerated by the stacking defects that propagate perpendicular to the sides of the rod. This results in stripes of  $Cu_{2-x}Te$  separating irregularly shaped areas of  $Cu_{2-x}S$ . This propagation direction is parallel to the hexagonally close-packed planes of anions and the cation layers, as the exchange is promoted by the defects in stacking

of the  $\{001\}$  weissite planes. Such formation of  $Cu_{2-x}Te$ stripes is, therefore, consistent with the enhanced mobility of the anions within these layers of the pseudohexagonal Cu<sub>2-x</sub>S crystal after initiation at a point on the surface. It is also consistent with the finding that sequential cation exchange preferentially targets interfaces where crystallinity has been disrupted. In the third stage, increased temperature drives increased crystallinity and coalescence of the remaining irregularly distributed Cu<sub>2-x</sub>S domains into two cores (rarely into one). The resulting heterostructure is similar to the rods occasionally observed due to the partial cation exchange of PbSe with Cd<sup>2+,60</sup> This behavior could be attributed to coalescence to decrease the interfacial energy or faster consumption of small  $Cu_{2-x}S$  domains at higher temperatures. However, the consistent observation of the two domains, each roughly one-quarter of the length of the rod from each end, implies a coalescence process in which sulfide ions diffuse to the core. Similar interface-driven phase segregation has been observed to create stripes, not embedded cores, along the rods in partial cation exchange. <sup>2,44,61</sup> The number (one or two) and relative size of the cores vary because they are dependent on the initial, randomly placed exchange-initiating defects. S<sup>2-</sup> in these irregular areas would coalesce into the nearest core. Phase segregation into two cores roughly placed one-quarter and three-fourths of the rod length from the tips is due to the limited diffusion lengths of  $S^{2-}$  parallel to the rods.

## 4. CONCLUSIONS

Exemplifying the power of postsynthetic NP transformation as a means for the rational design of nanoheterostructures, Cu<sub>2-x</sub>S nanorods are reliable synthons enabling a large variety of complex heterostructures through multigeneration cation exchange. 1,8 Introduction of anion exchange with variability in extent and regioselectivity of replacement greatly increases the possibilities for more complex heterostructures. It also expands the avenues for detailing the interplay between cation and anion exchange in the design of NPs and exploration of the emergent properties of such systems. Here, we demonstrated that the regioselectivity of anion exchange with tellurium to form weissite Cu<sub>2-x</sub>Te results in three distinct stages. Initially, near-isotropic exchange produces a core/shell Cu<sub>2-x</sub>S/  $Cu_{2-x}$ Te structure. As exchange proceeds preferentially parallel to the pseudohexagonally close-packed planes of the anion sublattice due to stacking defects, irregular patches of Cu<sub>2-x</sub>S within  $Cu_{2-x}$ Te result. These  $Cu_{2-x}$ S domains finally coalesce into a double-core structure. Elucidating this stepwise transformation process, which occurs while maintaining the nanorod morphology despite the necessary disruption of the anion sublattice, opens avenues to create many new mixed chalcogenide nanoheterostructures. Uncovering synthetic strategies for inducing or avoiding the Kirkendall effect moves the field closer toward a priori design of NP morphology.

# ASSOCIATED CONTENT

#### Supporting Information

The Supporting Information is available free of charge at https://pubs.acs.org/doi/10.1021/acs.chemmater.1c01107.

EDS spectra of unexchanged and near-fully exchanged nanorods; comparison of the  $\alpha$ -chalcocite and weissite crystal structures; structure comparisons between  $\alpha$ -chalcocite and roxbyite and its effect on anion exchange;

copper telluride crystal structure assignment; and microscopy data (PDF)

## AUTHOR INFORMATION

## **Corresponding Author**

Katherine E. Plass — Department of Chemistry, Franklin & Marshall College, Lancaster 17604, Pennsylvania, United States; ocid.org/0000-0002-4544-5471; Email: kplass@fandm.edu

## **Authors**

Luis F. Garcia-Herrera — Department of Chemistry, Franklin & Marshall College, Lancaster 17604, Pennsylvania, United States; occid.org/0000-0003-0905-9087

Haley P. McAllister — Department of Chemistry, Franklin & Marshall College, Lancaster 17604, Pennsylvania, United States; orcid.org/0000-0002-1522-1311

Huiyan Xiong – Department of Chemistry, Franklin & Marshall College, Lancaster 17604, Pennsylvania, United States; oorcid.org/0000-0002-3742-4769

Haiying Wang — Materials Characterization Laboratory, The Pennsylvania State University, University Park 16802, Pennsylvania, United States

Robert W. Lord — Department of Chemistry, The Pennsylvania State University, University Park 16802, Pennsylvania, United States; © orcid.org/0000-0003-1487-1598

Sarah K. O'Boyle – Department of Chemistry, The Pennsylvania State University, University Park 16802, Pennsylvania, United States; orcid.org/0000-0001-8341-9891

Adem Imamovic — Department of Chemistry, Franklin & Marshall College, Lancaster 17604, Pennsylvania, United States; © orcid.org/0000-0001-5590-9084

Benjamin C. Steimle — Department of Chemistry, The Pennsylvania State University, University Park 16802, Pennsylvania, United States; orcid.org/0000-0003-3398-8038

Raymond E. Schaak – Department of Chemistry, Department of Chemical Engineering, Materials Research Institute, The Pennsylvania State University, University Park 16802, Pennsylvania, United States

Complete contact information is available at: https://pubs.acs.org/10.1021/acs.chemmater.1c01107

#### **Funding**

This work was supported by Franklin & Marshall College through faculty and student grants and by student support via the Marshall Fellows Program (HPM) and the Committee on Grants; the Henry Dreyfus Teacher-Scholar award (TH-16-010); and the U.S. National Science Foundation through DMR-2003337 and instrument support (EAR-0923224 and CHE-1724948). R.S. acknowledges support from the U.S. National Science Foundation under grant DMR-1904122.

## Notes

The authors declare no competing financial interest.

#### ACKNOWLEDGMENTS

We acknowledge the useful conversations with Katelyn Baumler, Auston Butterfield, Connor McCormick, and Abigail Fagan as well as the support of the Materials Characterization Laboratory at the Pennsylvania State University.

#### ABBREVIATIONS

TOP, trioctylphosphine; Te=TOP, tellurium-trioctylphosphine complex

# REFERENCES

- (1) Steimle, B. C.; Fenton, J. L.; Schaak, R. E. Rational Construction of a Scalable Heterostructured Nanorod Megalibrary. *Science* **2020**, 367, 418–424.
- (2) Robinson, R. D.; Sadtler, B.; Demchenko, D. O.; Erdonmez, C. K.; Wang, L.-W.; Alivisatos, A. P. Spontaneous Superlattice Formation in Nanorods through Partial Cation Exchange. *Science* **2007**, *317*, 355–358.
- (3) Liu, Y.; Lim, C.-K.; Fu, Z.; Yin, D.; Swihart, M. T. Can the Morphology of Biconcave Metal Sulfide Nanoplatelets Be Preserved during Cation Exchange? *Chem. Mater.* **2019**, *31*, 5706–5712.
- (4) Liu, Y.; Liu, M.; Yin, D.; Qiao, L.; Fu, Z.; Swihart, M. T. Selective Cation Incorporation into Copper Sulfide Based Nanoheterostructures. *ACS Nano* **2018**, *12*, 7803–7811.
- (5) Lesnyak, V.; George, C.; Genovese, A.; Prato, M.; Casu, A.; Ayyappan, S.; Scarpellini, A.; Manna, L. Alloyed Copper Chalcogenide Nanoplatelets via Partial Cation Exchange Reactions. *ACS Nano* **2014**, *8*, 8407–8418.
- (6) Li, H.; Zanella, M.; Genovese, A.; Povia, M.; Falqui, A.; Giannini, C.; Manna, L. Sequential Cation Exchange in Nanocrystals: Preservation of Crystal Phase and Formation of Metastable Phases. *Nano Lett.* **2011**, *11*, 4964–4970.
- (7) Le, H. K. D.; Xiong, H.; Page, B. A.; Garcia-Herrera, L. F.; McAllister, H. P.; Li, B. C.; Wang, H.; Plass, K. E. Effects of I2 on Cu2-xS Nanoparticles: Enabling Cation Exchange but Complicating Plasmonics. ACS Mater. Lett. 2020, 2, 140–146.
- (8) Fenton, J. L.; Steimle, B. C.; Schaak, R. E. Tunable Intraparticle Frameworks for Creating Complex Heterostructured Nanoparticle Libraries. *Science* **2018**, *360*, 513–517.
- (9) Macdonald, T. J.; Mange, Y. J.; Dewi, M.; McFadden, A.; Skinner, W. M.; Nann, T. Cation exchange of aqueous CuInS2 quantum dots. *CrystEngComm* **2014**, *16*, 9455–9460.
- (10) Son, D. H.; Hughes, S. M.; Yin, Y.; Paul Alivisatos, A. Cation Exchange Reactions in Ionic Nanocrystals. *Science* **2004**, *306*, 1009–1012.
- (11) Beberwyck, B. J.; Surendranath, Y.; Alivisatos, A. P. Cation Exchange: A Versatile Tool for Nanomaterials Synthesis. *J. Phys. Chem. C* **2013**, *117*, 19759–19770.
- (12) Lesnyak, V.; Brescia, R.; Messina, G. C.; Manna, L. Cu Vacancies Boost Cation Exchange Reactions in Copper Selenide Nanocrystals. *J. Am. Chem. Soc.* **2015**, *137*, 9315–9323.
- (13) Akkerman, Q. A.; Genovese, A.; George, C.; Prato, M.; Moreels, I.; Casu, A.; Marras, S.; Curcio, A.; Scarpellini, A.; Pellegrino, T.; et al. From Binary Cu2S to Ternary Cu-In-S and Quaternary Cu-In-Zn-S Nanocrystals with Tunable Composition via Partial Cation Exchange. ACS Nano 2015, 9, 521–531.
- (14) Gariano, G.; Lesnyak, V.; Brescia, R.; Bertoni, G.; Dang, Z.; Gaspari, R.; De Trizio, L.; Manna, L. Role of the Crystal Structure in Cation Exchange Reactions Involving Colloidal Cu2Se Nanocrystals. *J. Am. Chem. Soc.* **2017**, *139*, 9583–9590.
- (15) Powell, A. E.; Hodges, J. M.; Schaak, R. E. Preserving Both Anion and Cation Sublattice Features during a Nanocrystal Cation-Exchange Reaction: Synthesis of Metastable Wurtzite-Type CoS and MnS. J. Am. Chem. Soc. 2016, 138, 471–474.
- (16) Fenton, J. L.; Steimle, B. C.; Schaak, R. E. Exploiting Crystallographic Regioselectivity To Engineer Asymmetric Three-Component Colloidal Nanoparticle Isomers Using Partial Cation Exchange Reactions. J. Am. Chem. Soc. 2018, 140, 6771–6775.
- (17) Wang, X.; Liu, X.; Zhu, D.; Swihart, M. T. Controllable conversion of plasmonic Cu2–xS nanoparticles to Au2S by cation exchange and electron beam induced transformation of Cu2–xS-Au2S core/shell nanostructures. *Nanoscale* **2014**, *6*, 8852–8857.

- (18) Saruyama, M.; Sato, R.; Teranishi, T. Transformations of Ionic Nanocrystals via Full and Partial Ion Exchange Reactions. *Acc. Chem. Res.* **2021**, *54*, 765–775.
- (19) Li, X.; Ji, M.; Li, H.; Wang, H.; Xu, M.; Rong, H.; Wei, J.; Liu, J.; Liu, J.; Chen, W.; et al. Cation/Anion Exchange Reactions toward the Syntheses of Upgraded Nanostructures: Principles and Applications. *Matter* **2020**, *2*, 554–586.
- (20) Cho, G.; Park, Y.; Hong, Y.-K.; Ha, D.-H. Ion Exchange: An Advanced Synthetic Method for Complex Nanoparticles. *Nano Convergence* **2019**, *6*, 17.
- (21) Parobek, D.; Dong, Y.; Qiao, T.; Rossi, D.; Son, D. H. Photoinduced Anion Exchange in Cesium Lead Halide Perovskite Nanocrystals. *J. Am. Chem. Soc.* **2017**, *139*, 4358–4361.
- (22) Koscher, B. A.; Bronstein, N. D.; Olshansky, J. H.; Bekenstein, Y.; Alivisatos, A. P. Surface- vs Diffusion-Limited Mechanisms of Anion Exchange in CsPbBr3 Nanocrystal Cubes Revealed through Kinetic Studies. *J. Am. Chem. Soc.* **2016**, *138*, 12065–12068.
- (23) Creutz, S. E.; Crites, E. N.; De Siena, M. C.; Gamelin, D. R. Anion Exchange in Cesium Lead Halide Perovskite Nanocrystals and Thin Films Using Trimethylsilyl Halide Reagents. *Chem. Mater.* **2018**, 30, 4887–4891.
- (24) Nedelcu, G.; Protesescu, L.; Yakunin, S.; Bodnarchuk, M. I.; Grotevent, M. J.; Kovalenko, M. V. Fast Anion-Exchange in Highly Luminescent Nanocrystals of Cesium Lead Halide Perovskites (CsPbX3, X = Cl, Br, I). *Nano Lett.* **2015**, *15*, 5635–5640.
- (25) Draguta, S.; Sharia, O.; Yoon, S. J.; Brennan, M. C.; Morozov, Y. V.; Manser, J. S.; Kamat, P. V.; Schneider, W. F.; Kuno, M. Rationalizing the Light-Induced Phase Separation of Mixed Halide Organic-Inorganic Perovskites. *Nat. Commun.* **2017**, *8*, 200.
- (26) Hoke, E. T.; Slotcavage, D. J.; Dohner, E. R.; Bowring, A. R.; Karunadasa, H. I.; McGehee, M. D. Reversible Photo-Induced Trap Formation in Mixed-Halide Hybrid Perovskites for Photovoltaics. *Chem. Sci.* **2015**, *6*, 613–617.
- (27) Park, J.; Zheng, H.; Jun, Y.-w.; Alivisatos, A. P. Hetero-Epitaxial Anion Exchange Yields Single-Crystalline Hollow Nanoparticles. *J. Am. Chem. Soc.* **2009**, *131*, 13943–13945.
- (28) Hodges, J. M.; Kletetschka, K.; Fenton, J. L.; Read, C. G.; Schaak, R. E. Sequential Anion and Cation Exchange Reactions for Complete Material Transformations of Nanoparticles with Morphological Retention. *Angew. Chem., Int. Ed. Engl.* **2015**, *54*, 8669–8672.
- (29) Fenton, J. L.; Fagan, A. M.; Schaak, R. E. General Solution-Phase Synthesis of Nanoscale Transition Metal Tellurides Using Metal Nanoparticle Reagents. *Eur. J. Inorg. Chem.* **2019**, 2019, 3490–3493.
- (30) Saruyama, M.; So, Y.-G.; Kimoto, K.; Taguchi, S.; Kanemitsu, Y.; Teranishi, T. Spontaneous Formation of Wurzite-CdS/Zinc Blende-CdTe Heterodimers through a Partial Anion Exchange Reaction. J. Am. Chem. Soc. 2011, 133, 17598–17601.
- (31) Han, C.; Bai, Y.; Sun, Q.; Zhang, S.; Li, Z.; Wang, L.; Dou, S. Ambient Aqueous Growth of Cu 2 Te Nanostructures with Excellent Electrocatalytic Activity toward Sulfide Redox Shuttles. *Adv. Sci.* **2016**, 3, 1500350.
- (32) Sines, I. T.; Vaughn, D. D.; Biacchi, A. J.; Kingsley, C. E.; Popczun, E. J.; Schaak, R. E. Engineering Porosity into Single-Crystal Colloidal Nanosheets Using Epitaxial Nucleation and Chalcogenide Anion Exchange Reactions: The Conversion of SnSe to SnTe. Chem. Mater. 2012, 24, 3088–3093.
- (33) Lim, Y.; Lee, C.-H.; Jun, C.-H.; Kim, K.; Cheon, J. Morphology-Conserving Non-Kirkendall Anion Exchange of Metal Oxide Nanocrystals. *J. Am. Chem. Soc.* **2020**, *142*, 9130–9134.
- (34) Yang, Z.; Yang, N.; Pileni, M.-P. Nano Kirkendall Effect Related to Nanocrystallinity of Metal Nanocrystals: Influence of the Outward and Inward Atomic Diffusion on the Final Nanoparticle Structure. *J. Phys. Chem. C* **2015**, *119*, 22249–22260.
- (35) Jia, B.; Zhao, W.; Sun, D.; Fan, L.; Yao, H.; Lu, P.; Xu, F.; Huang, F. Robust Anion Exchange Realized in Crystalline Metal Cyanamide Nanoparticles. *Chem. Mater.* **2019**, *31*, 9532–9539.

- (36) Xie, Y.; Qian, Y.; Zhang, S.; Xie, Y.; Yan, P.; Lu, J. CdS/CdSe Core/Sheath Nanostructures Obtained from CdS Nanowires. *Chem. Commun.* **1999**, 1969–1970.
- (37) Dawood, F.; Schaak, R. E. ZnO-Templated Synthesis of Wurtzite-Type ZnS and ZnSe Nanoparticles. *J. Am. Chem. Soc.* **2009**, 131, 424–425.
- (38) Wang, Y.; Liu, M.-X.; Ling, T.; Tang, C.-C.; Zhi, C.-Y.; Du, X.-W. Gas-Phase Anion Exchange towards ZnO/ZnSe Heterostructures with Intensive Visible Light Emission. *J. Mater. Chem. C* **2014**, 2, 2793–2798.
- (39) Huang, X.; Wang, M.; Willinger, M.-G.; Shao, L.; Su, D. S.; Meng, X.-M. Assembly of Three-Dimensional Hetero-Epitaxial ZnO/ZnS Core/Shell Nanorod and Single Crystalline Hollow ZnS Nanotube Arrays. *ACS Nano* **2012**, *6*, 7333–7339.
- (40) Geng, J.; Liu, B.; Xu, L.; Hu, F.-N.; Zhu, J.-J. Facile Route to Zn-Based II—VI Semiconductor Spheres, Hollow Spheres, and Core/Shell Nanocrystals and Their Optical Properties. *Langmuir* **2007**, 23, 10286—10293.
- (41) De Trizio, L.; Manna, L. Forging Colloidal Nanostructures via Cation Exchange Reactions. *Chem. Rev.* **2016**, *116*, 10852–10887.
- (42) Tu, R.; Xie, Y.; Bertoni, G.; Lak, A.; Gaspari, R.; Rapallo, A.; Cavalli, A.; De Trizio, L.; Manna, L. Influence of the Ion Coordination Number on Cation Exchange Reactions with Copper Telluride Nanocrystals. *J. Am. Chem. Soc.* **2016**, *138*, 7082–7090.
- (43) Ha, D.-H.; Caldwell, A. H.; Ward, M. J.; Honrao, S.; Mathew, K.; Hovden, R.; Koker, M. K. A.; Muller, D. A.; Hennig, R. G.; Robinson, R. D. Solid-Solid Phase Transformations Induced through Cation Exchange and Strain in 2D Heterostructured Copper Sulfide Nanocrystals. *Nano Lett.* **2014**, *14*, 7090–7099.
- (44) Sadtler, B.; Demchenko, D. O.; Zheng, H.; Hughes, S. M.; Merkle, M. G.; Dahmen, U.; Wang, L.-W.; Alivisatos, A. P. Selective Facet Reactivity during Cation Exchange in Cadmium Sulfide Nanorods. *J. Am. Chem. Soc.* **2009**, *131*, 5285–5293.
- (45) Willhammar, T.; Sentosun, K.; Mourdikoudis, S.; Goris, B.; Kurttepeli, M.; Bercx, M.; Lamoen, D.; Partoens, B.; Pastoriza-Santos, I.; Pérez-Juste, J.; et al. Structure and Vacancy Distribution in Copper Telluride Nanoparticles Influence Plasmonic Activity in the Near-Infrared. *Nat. Commun.* **2017**, *8*, 14925.
- (46) Kriegel, I.; Rodríguez-Fernández, J.; Wisnet, A.; Zhang, H.; Waurisch, C.; Eychmüller, A.; Dubavik, A.; Govorov, A. O.; Feldmann, J. Shedding Light on Vacancy-Doped Copper Chalcogenides: Shape-Controlled Synthesis, Optical Properties, and Modeling of Copper Telluride Nanocrystals with near-Infrared Plasmon Resonances. ACS Nano 2013, 7, 4367–4377.
- (47) Kriegel, I.; Jiang, C.; Rodríguez-Fernández, J.; Schaller, R. D.; Talapin, D. V.; da Como, E.; Feldmann, J. Tuning the Excitonic and Plasmonic Properties of Copper Chalcogenide Nanocrystals. *J. Am. Chem. Soc.* **2012**, *134*, 1583–1590.
- (48) He, Y.; Zhang, T.; Shi, X.; Wei, S.-H.; Chen, L. High Thermoelectric Performance in Copper Telluride. *NPG Asia Mater.* **2015**, *7*, No. e210.
- (49) Nethravathi, C.; Rajamathi, C. R.; Rajamathi, M.; Maki, R.; Mori, T.; Golberg, D.; Bando, Y. Synthesis and Thermoelectric Behaviour of Copper Telluride Nanosheets. *J. Mater. Chem. A* **2014**, 2, 985–990.
- (50) He, Y.; Day, T.; Zhang, T.; Liu, H.; Shi, X.; Chen, L.; Snyder, G. J. High Thermoelectric Performance in Non-Toxic Earth-Abundant Copper Sulfide. *Adv. Mater.* **2014**, *26*, 3974–3978.
- (51) Kruszynska, M.; Borchert, H.; Bachmatiuk, A.; Rümmeli, M. H.; Büchner, B.; Parisi, J.; Kolny-Olesiak, J. Size and Shape Control of Colloidal Copper(I) Sulfide Nanorods. *ACS Nano* **2012**, *6*, 5889–5896.
- (52) Yu, L.; Luo, K.; Chen, S.; Duan, C.-G. Cu-deficiency induced structural transition of Cu2-xTe. *CrystEngComm* **2015**, *17*, 2878–2885.
- (53) Nelson, A.; Ha, D.-H.; Robinson, R. D. Selective Etching of Copper Sulfide Nanoparticles and Heterostructures through Sulfur Abstraction: Phase Transformations and Optical Properties. *Chem. Mater.* **2016**, 28, 8530–8541.

- (54) Fenton, J. L.; Schaak, R. E. Structure-Selective Cation Exchange in the Synthesis of Zincblende MnS and CoS Nanocrystals. *Angew. Chem., Int. Ed. Engl.* **2017**, *56*, 6464–6467.
- (55) Butterfield, A. G.; Alameda, L. T.; Schaak, R. E. Emergence and Control of Stacking Fault Formation during Nanoparticle Cation Exchange Reactions. *J. Am. Chem. Soc.* **2021**, *143*, 1779–1783.
- (56) Moon, G. D.; Min, Y.; Ko, S.; Kim, S.-W.; Ko, D.-H.; Jeong, U. Understanding the Epitaxial Growth of SexTey@Te Core—Shell Nanorods and the Generation of Periodic Defects. *ACS Nano* **2010**, *4*, 7283—7292.
- (57) Shannon, R. D. Revised Effective Ionic Radii and Systematic Studies of Interatomic Distances in Halides and Chalcogenides. *Acta Crystallogr. Sect. A Cryst. Phys. Diffr. Theor. Gen. Crystallogr.* **1976**, 32, 751–767.
- (58) Landry, C. C.; Lockwood, J.; Barron, A. R. Synthesis of Chalcopyrite Semiconductors and Their Solid Solutions by Microwave Irradiation. *Chem. Mater.* **1995**, *7*, 699–706.
- (59) Saldanha, P. L.; Brescia, R.; Prato, M.; Li, H.; Povia, M.; Manna, L.; Lesnyak, V. Generalized One-Pot Synthesis of Copper Sulfide, Selenide-Sulfide, and Telluride-Sulfide Nanoparticles. *Chem. Mater.* **2014**, *26*, 1442–1449.
- (60) Casavola, M.; van Huis, M. A.; Bals, S.; Lambert, K.; Hens, Z.; Vanmaekelbergh, D.; Vanmaekelbergh, D. Anisotropic Cation Exchange in PbSe/CdSe Core/Shell Nanocrystals of Different Geometry. *Chem. Mater.* **2012**, *24*, 294–302.
- (61) Demchenko, D. O.; Robinson, R. D.; Sadtler, B.; Erdonmez, C. K.; Alivisatos, A. P.; Wang, L.-W. Formation Mechanism and Properties of CdS-Ag2S Nanorod Superlattices. *ACS Nano* **2008**, *2*, 627–636.